TAMPEREEN TEKNILLINEN YLIOPISTO
TAMPERE UNIVERSITY OF TECHNOLOGY

MARTTI LEINO

ALPHA RADIATION DETECTION METHODS USING RADIOLUMINESCENCE OF AIR

Bachelor of Science thesis

Examiner: Prof. Juha Toivonen

ABSTRACT

MARTTI LEINO: Alpha Radiation Detection Methods Using Radioluminescence of Air
Tampere University of Technology
Bachelor of Science thesis, 25 pages
4th of February, 2019
Bachelor's Degree Programme in Engineering and Natural Sciences
Major: Engineering Physics
Examiner: Prof. Juha Toivonen
Keywords: radioluminescence, optical detection of alpha emitters, stand-off detection of alpha emitters, air fluorescence, minimum detectable activity

Many solutions have been demonstrated for utilizing radioluminescence for alpha radiation detection, enabling long range detection of radiation sources. This thesis examines the performance of two novel approaches for radioluminescence imaging. PMT Scanner based on a photomultiplier tube, telescope optics and a pan-tilt system and an intensified charge coupled device (ICCD) coupled with an UV-transmissive lens are compared in different measurement conditions with different measurement parameters by simulating their performance. Simulations are based on results of previous studies demonstrating the use of the two technologies.

Results of the simulation indicate that the PMT Scanner is the preferable technology in most measurement settings, as it is able to resolve similar activities in shorter measurement time than the ICCD camera. However, with improved optics, the ICCD camera is found to have comparable performance to the PMT Scanner, assuming that the measurement area is conducted in dark environment. If the minimum detectable activity of a measurement is required to be less than 8 kBq, the ICCD camera is determined to be the faster measurement technology. For activities higher than 8 kBq, the PMT Scanner is able to conduct the measurement in shorter time than the ICCD camera for similarly sized measurement area. The measurement conditions should be considered when deciding between the technologies, as the ICCD camera can not be operated in illuminated environments.

Measurements should still be conducted to study and improve the accuracy of the simulation. However, based on the results, it can be noted that new optics with better efficiency would increase the performance of the ICCD camera significantly. Deployment of the ICCD camera could be simplified by developing practical solutions for achieving sufficient light shielding. Performance of the PMT Scanner could be enhanced by optimizing the field of view of the optics.

CONTENTS

LIST OF ABBREVIATIONS AND SYMBOLS

CCD	charge-coupled device
DAQ	data acquisition
FOW	field of view
ICCD	intensified charge coupled device
MCP	micro channel plate
MDA	minimum detectable activity
PMT	photomultiplier tube
SDD	source-to-detector distance
SNR	signal-to-noise ratio
UV	ultraviolet

η_{pc}	photocathode quantum efficiency
θ	angular width of scan area
φ	angular height of scan area
Ω	geometrical efficiency
A_{eff}	effective aperture diameter
A_s	activity of radiation source
F_m	MCP noise factor
L_D	net signal level
M	atomic mass
N	noise level
N_B	background count rate
N_{EBI}	equivalent background illumination
N_s	signal count rate
P	photon flux per pixel
p	momentum
Q	decay energy
R	angular resolution
S	signal level
t_tot	total measurement time
t_m	movement time
t_i	integration time

1. INTRODUCTION

Globally, more than 400 nuclear power reactors require dismantling efforts on the coming decades. Cost for decommissioning these facilities has been estimated to be in excess of $180 billion between 2001 and 2050. Total costs of decommissioning of all types of nuclear facilities for the same period is more than $900 billion. [9] One of the challenges faced during the decommissioning process is surveying the radiation levels and types before and during the dismantling of the facilities.

Current alpha radiation detection instruments require the source-to-detector distance (SDD) to be 1 cm or shorter [10]. Due to the limitation of detection distance, inspecting large areas for alpha contamination is time consuming. Moreover, personnel conducting the inspections are exposed to ionizing radiation during the scanning process, and extensive measures for avoiding contamination must be taken. Novel, optical methods based on a radioluminescence of air near the alpha radiation sources have been demonstrated for detecting alpha contamination [13, 19, 20, 21]. Aim of these methods is to simplify the measurement process by enabling considerably longer SDD than the conventional detection methods.

In this thesis, the performance of two optical detector technologies for alpha radiation detection are compared: Photomultiplier Tube (PMT) Scanner [21] and an intensified charge coupled device (ICCD) camera with an ultraviolet (UV) transmissive objective [20]. The PMT Scanner is able to conduct measurements in illuminated environments, requiring that the measurement band ranging from 330 nm to 350 nm is free of background illumination. Sources with activities down to 4.2 kBq have been demonstrated to be resolvable with the scanner. [21] ICCD camera has been used to image a 2.79 MBq source [20]. The aim of this work was to determine the preferable technology for different measurement conditions by simulating the effects of SDD and other parameters on the performance of the systems.

This thesis consists of six chapters. First, theoretical background of alpha radiation and radioluminescence are described, followed by an overview of the detector and filter technologies used in the devices. After the device configurations, limitations and features affecting the time requirement and performance of the technologies are

compared, and literature results used as the basis of the simulations are presented. In the Performance Analysis, methodology and results of the simulations are presented, and the performances of the systems are compared. Lastly, the relevance of the results and most significant developement areas are discussed.

2. ALPHA RADIATION AND RADIOLUMINESCENCE

Optical detection of alpha radiation is based on radioluminescence, in which kinetic energy of the alpha particle gets converted to electromagnetic radiation. In this section, phenomena of alpha radiation and radioluminescence are explained.

2.1 Alpha Radiation

Alpha radiation is a type of ionizing radiation produced mainly in nuclear reactions. It's ionizing nature makes it harmful for living organisms by causing damage to cells and DNA. Due to it's large stopping power and short range in medium alpha radiation is considered to be more harmful for living organisms than beta or gamma radiation when consumed internally.

Alpha particle consists of two protons and two neutrons. Alpha radiation is produced when an alpha particle is emitted from radioactive nucleus. Chemical equation for alpha decay is

$$ {}^{A}_{Z}P \longrightarrow {}^{A-4}_{Z-2}D + \alpha, \tag{2.1} $$

where P is the parent nucleus, D is the daughter nucleus, A is the mass number and Z is the atomic number of the parent nucleus. Q, the energy released in the decay process can be calculated from the difference in total mass of the parent nucleus when compared to the decay products:

$$ \frac{Q}{c^2} = M_P - (M_D + M_{He}), \tag{2.2} $$

where M_P, M_D and are the masses of the parent and daughter atoms. M_{He} is the mass of the helium atom. Atom masses rather than nucleus masses are used so that the masses of the electrons cancel out. [24]

Due to the conservation of momentum, some of the decay energy is transferred to the daughter nucleus. The decay energy can be written as

$$Q = \frac{p^2}{2M_{He}}\left(1 + \frac{M_{He}}{M_D}\right) \tag{2.3}$$

where p is the magnitude of the momentum of the daughter nucleus and the alpha particle. Energy of the alpha particle can now be written as

$$E_\alpha = \frac{p^2}{2M_{He}} = \frac{A-4}{A}Q \tag{2.4}$$

Alpha particle is the heaviest of the nuclear decay products, others being . It has also the biggest electric charge. Due to these factors, it thermalizes in relatively short distance in medium. Thermalization distance in air, for example, is about 4 cm.

2.2 Alpha-Induced Air Radioluminescence

Radioluminescence is a phenomenon in which some of the kinetic energy of the radioactive decay products get converted into electromagnetic radiation. The effect was discovered by Sir William and Lady Huggins in 1903 [8]. Radioluminescence is most notable with alpha particles due to their relatively large stopping power and short range in air. Most of the kinetic energy of the particle is lost in the vicinity of the radiation source, which also means that the majority of the radioluminescence is produced near the source. In contrary, radioluminescence of beta and gamma radiation originates from a larger volume around a source due to their longer range in air.

Few experiments have been made to determine the yield of radioluminescence photons of alpha particles. Analysis conducted by Bachelor et al. suggests that the conversion efficiency of alpha particle's kinetic energy to UV-photons is $1.3 * 10^{-5}$ in normal atmosphere [2]. In another study conducted by Baschenco the conversion efficiency was found to be $2.5 * 10^{-5}$ and that on average 30 photons would be generated by one alpha particle [3]. This translates to about 5.8 photons generated for 1 MeV of alpha radiation energy. In one of the most recent studies, Sand et al. measured the conversion efficiency to be $6.7 * 10^{-5}$ and 19 $\pm$3 photons to be created for each MeV of alpha particle kinetic energy [17].

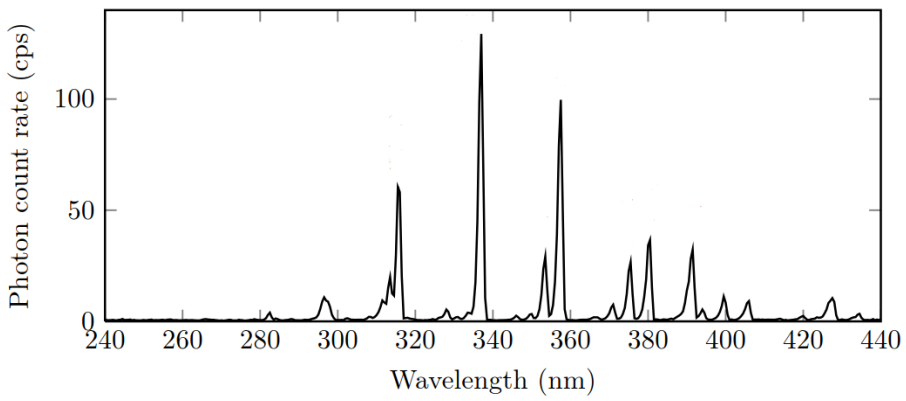

Figure 2.1 *Spectrum of air radioluminescence excited by alpha particles from Am-241. [18]*

Results of Sand et al. for the alpha particle yield are higher than previous experiments would suggest. However, the results are in good agreement with yield predicted by a computer model developed by Thompson et al. with Geant4 framework [23]. Spectrum of air radioluminescence is shown in Figure 2.1. They also note that the yields are similar to results of studies done with electron beams of energies from 0.85 MeV to 50 GeV. Therefore, it seems reasonable to conclude that roughly 19 photons are generated per MeV of alpha energy in normal atmosphere.

Radioluminescence yield can be increased by changing the composition of the atmosphere surrounding the radioactive material. Radioluminescence in atmosphere mostly originates from relaxation of 2P band of neutral N_2 and 1N band of N_2^+. Oxygen and water vapor contained in normal atmosphere are known to cause quenching of the excited states of nitrogen molecules. Nitrogen molecules cause also self-quenching of the excited states. Oxygen quenching plays the biggest role since it's concentration in air is much higher in normal circumstances compared to water vapor. [25]

In pure nitrogen, radioluminescence signal can be 6 times better than in normal atmosphere [17]. This is mostly due to the lack of oxygen and water vapor quenching. Introducing NO in to the nitrogen atmosphere is found to increase the net signal even more. The optimum concentration of NO in pure nitrogen is about 50 ppm, resulting in 150 fold increase in signal compared to normal air [12].

3. RADIOLUMINESCENCE SENSING TECHNOLOGIES

As discussed in Section 2.2, photon yield of radioluminescence is relatively low compared to background illumination levels in most measurement scenarios. This poses some requirements for the detector technology. The detector has to have low dark current and good collection and quantum efficiencies. Different approaches can be considered for detecting photons created in radioluminescence process. The two technologies examined in this section are a scanner device using a PMT as the detector and an ICCD camera coupled with an UV transmissive lens.

3.1 Photomultiplier tube

Discoveries of photoelectric effect and secondary electron emission in late 19th and early 20th century led to the invention of the photomultiplier tube. Although PMTs were invented more than 80 years ago, they are still widely used in biological and medical applications, as they offer low dark current and good quantum efficiency required for the detection of single photon signals. [16]

Detection process in PMT can be divided into 4 sub processes:

1. Emission of photoelectron from photocathode
2. Electron multiplication in electron multiplier
3. Collection of multiplied electrons on the anode
4. Detection of current signal with detection electronics

The first process, photoelectron emission from photocathode, largely determines the quantum efficiency of the PMT. For a photoelectron to be emitted, it has to get enough energy from the incident photon to overcome the vacuum level barrier of the photocathode material. [16]

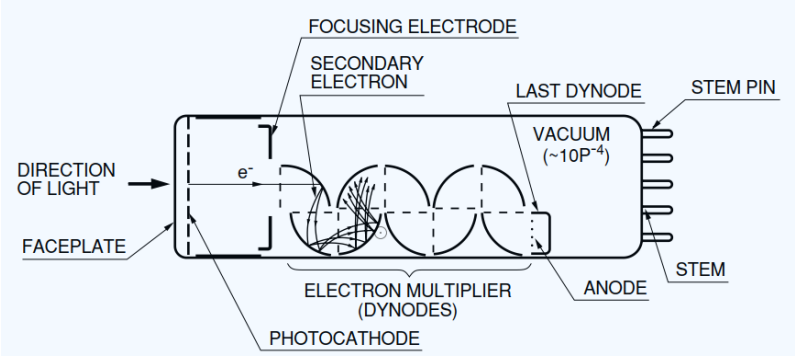

Figure 3.1 *Box-and-grid Type PMT. In transmission mode PMT, photons enter the photocathode from one side and photoelectrons are emitted from the opposite side. [7]*

Electron multiplier, which amplifies the electron signal from photocathode, consists of up to 20 dynodes. Large negative voltage is applied between consecutive dynodes which accelerates the electrons. In resulting collision, kinetic energy of the colliding electron is transferred to the electrons of the dynode material. As a result, more electrons get released from the dynode than originally landed on it. Amplification factor is typically between 10 and 100 for each dynode. [16]

After collecting the electrons on the anode output signal is compared with a threshold level in the detection electronics. This is necessary to filter out the dark current caused by thermal electrons that are emitted from the dynodes independent from photon signal. Current spike caused by the thermal electrons is usually lower than the signal originating from photocathode due to fewer dynode amplifications. [16]

3.2 Intensified Charge Coupled Device

Image intensifier tubes used in ICCD cameras were first developed for military applications, night vision devices in particular [4, cited in 6]. The intensification in the image intensifier happens in 3 main stages: emission of photoelectron on photocathode, electron multiplication and electron cloud formation in micro channel plate (MCP), and photon emission via phosphorescence on a phosphor screen after the electron multiplication.

Structure of intensifier tube is shown in Figure 3.2. Sensitivity of ICCD camera can be varied by changing the voltage B across the MCP. This is called gain voltage. One electron entering the MCP can create a cloud of 10^3 to 10^7 electrons depending on the MCP design [6]. Electron cloud formed in the MCP is then accelerated towards the phosphor screen where kinetic energy of the electrons is converted back to photons, which are then recorded with a CCD sensor. [1]

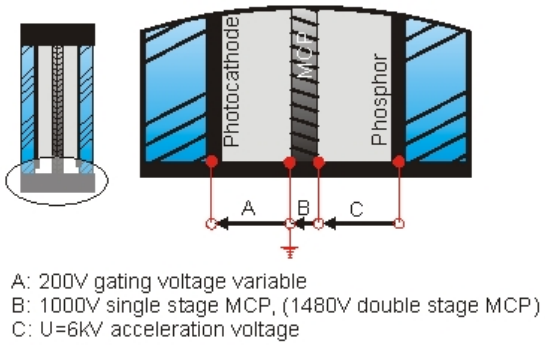

Figure 3.2 *Image intensifier of an ICCD camera [22]. Photons arrive to the photocathode from left, releasing electrons, which are then drawn to the MCP by a positive voltage. Multiplied electron from the MCP are accelerated to the phosphor screen with an acceleration voltage.*

Photocathode material determines the spectral response of the image intensifier. Vast variety of different photocathode materials are available from camera manufacturers. Good quantum efficiency in the UV-range and lower sensitivity in other wavelengths is the most important criteria when determining the best photocathode material for radioluminescence imaging.

3.3 Interference Filters

It is often advantageous to filter a light signal to single out the relevant and informative wavelengths. This is the case also for the radioluminescence imaging, as background illumination is often hard to reduce by other means in field environment. Interference filters are a good choice when good transmission in particular wavelength band and high attenuation of other wavelengths is required.

Light can be filtered with a pair of dielectric layers with different refractive indexes, first layer having higher refractive index than the second one. The filtering power can be increased by stacking together multiple such pairs of layers. As light encounters the stack, some of it gets reflected from the first interface with a phase shift of 1 π, as it is moving from a medium with lower optical density to a medium with higher optical density. If the thickness of each layer equals 1/4 of the wavelength of the light, reflection from the second interface has a phase shift of 1 π compared to the original light ray. As a result, the two reflected light rays are in same phase and experience constructive interference. [15] Such a stack is called quarter-wave mirror, or Bragg mirror, and only reflects light with a specific wavelength. The process is illustrated in Figure 3.3a. If the layer thickness is 1/2 of the wavelength of the incoming light, reflected waves interfere destructively, resulting in transmission of the light. Destructive interference is represented in Figure 3.3b.

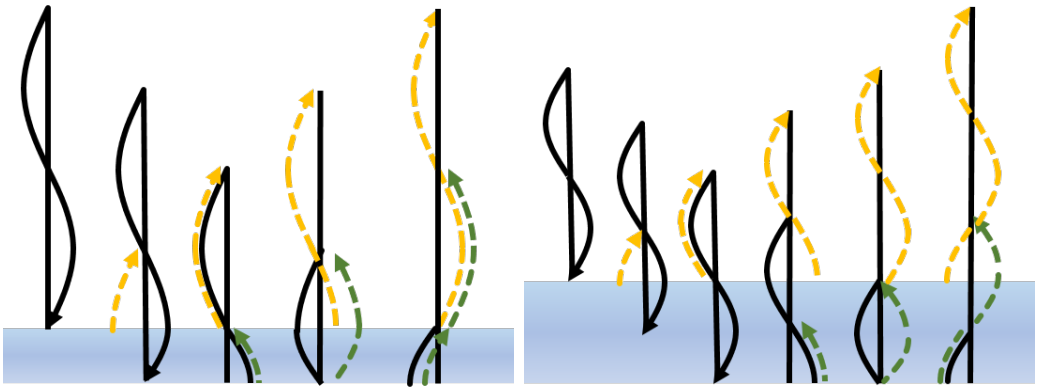

Figure 3.3 *Constructive (a) and destructive (b) interference process in interference filter. The steps are as follows: (1) light arrives to the interface separating two different substances. Some of the light enters the substance with higher refractive index and some gets reflected from the first interface with a phase shift of 1 π . (2) Light reflects from the second interface without phase shift. Yellow and green waves represent the light reflected from the first and second interface, respectively.*

By altering the layer thicknesses of the stack, mirrors with broader reflective bands can be designed, double-chirped mirrors being one example for the use of such a design [14]. With careful design and optimization, filters combining narrow transition bands, efficient transmission and high attenuation can be constructed. Filtering properties of interference filters are generally superior to other filter types. However, their sensitivity to changes in angle of incidence may cause difficulties in some applications.

4. EXPERIMENTAL ARRANGEMENTS

In this section two experimental arrangements, one utilizing photomultiplier tube and the other using intensified charge coupled device as the detector, are studied. Both technologies have been successfully used to detect radioluminescence signal. ICCD camera is readily capable of producing high resolution images of the measurement scene, while data collected with PMT Scanner requires post processing before visual presentation.

4.1 Photomultiplier tube Scanner

PMTs have been used for radioluminescence mapping with multiple experimental arrangements. Hand held Alpha UV Application [19] utilizing 2 PMTs was developed in Tampere University of Technology (TUT). Automated scanner devices developed for consistent mapping of larger areas have also been demonstrated by many research groups [11, 21]. This device, a PMT scanner, comprises of 6 main components:

1. Optics
2. Photomultiplier tube
3. Camera
4. Data acquisition (DAQ) card
5. Pan-tilt system
6. Control computer

Optics with narrow field of view (FOW) are used to collect the light produced by radioluminescence to the photon counting PMT. The optics are pointed to defined coordinates for a specific time, during which the counts from the PMT are recorded with a counter card. A pan-tilt system is used to move the optics between measurement points. A heat map is constructed from the measurement points by interpolation. The heat map is then superimposed on a normal image acquired with a small

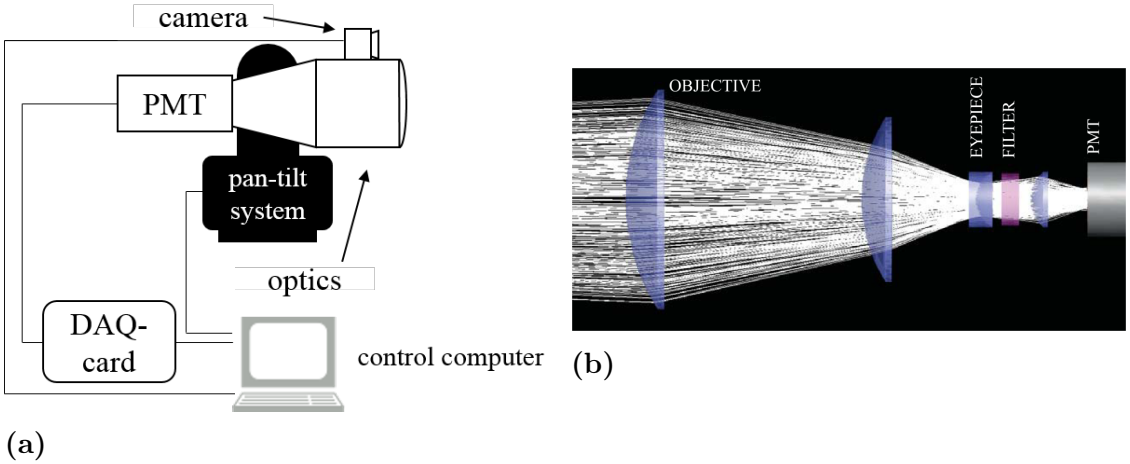

Figure 4.1 *(a) Diagram of the PMT scanner setup. Control computer is used to run the measurement sequence and to present the results. (b) PMT scanner optics design showing filter and lens layout. [21]*

camera attached on top of the scanner. The measurement sequence is constructed and performed by a control computer. System setup is shown in Figure 4.1a.

Optics designed for the scanner consist of a Galilean style telescope and a filter stack. Diameter of the telescope's main lens is 10 cm, which allows for good geometrical efficiency in the setup. FOW of the telescope is 2.5°, resulting in a circular image area with 8.7 cm diameter at 1 m distance. The lenses are manufactured from UV fused silica to allow better transmittance of UV wavelengths. Filter stacks can be compiled from standard filters with diameter of 25 mm. [21] Optical design of the telescope is shown in Figure 4.1b.

System was designed to be used in illuminated indoors environments and to have good sensitivity. These design objectives are best met when UV-free lighting is used for illumination. With this approach, the most intense parts of radioluminescence spectrum in air, particularly the spike in 335 nm, can be utilized for detection. An ultra bi-alkali PMT (H10682-210, Hamamatsu) with quantum efficiency of over 30 % for the specified 335 nm wavelength was chosen for the setup. [21] The Hamamatsu PMT is responsive to light with wavelengths ranging from 230 nm to 700 nm. Therefore, filters must be used to attenuate the unwanted wavelengths. Filter stack of three Semrock Inc FF01-335/7-25 filters was used to achieve desired attenuation while still providing high transmittance on the wavelengths with highest radioluminescence signal. [21]

Graphical user interface was developed for the PMT scanner to allow fast and easy operation of the system in field environment. Controlling of the pan-tilt system and reading the counter card are also managed by the program. Measurements are

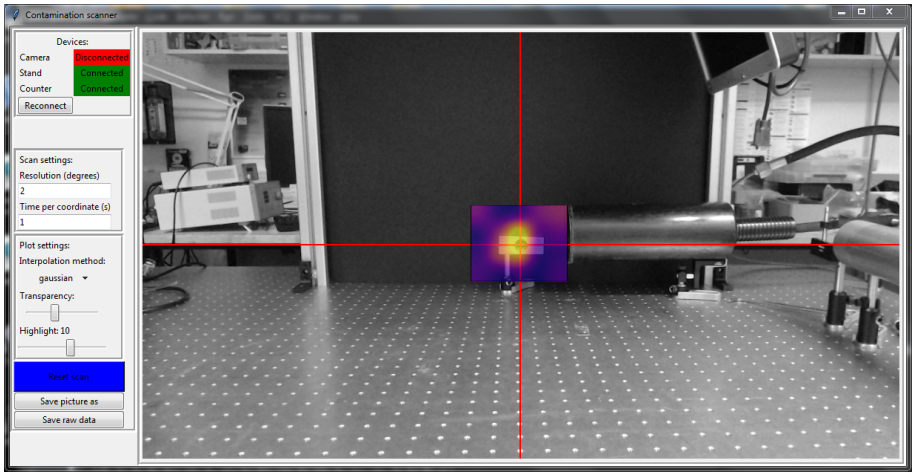

Figure 4.2 *Graphical user interface of the PMT Scanner. Heat map superimposed on a reference picture from the camera is presented on the right. Parameters for the measurement and heat map can be adjusted with the controls on the left side of the window.*

presented to the user as a heat map superimposed on a black and white image from the camera for spatial reference. Graphical user interface and result of measurement are shown in Figure 4.2. Threading is utilized in the program design to allow continuous real-time updating of the radioluminescence heat map and interaction with the user. Both, the raw data and the radiation heat map can be saved for later examination.

Yellow fluorescent tube emitting little light below wavelengths 500 nm was used for illumination during measurement. Three alpha emitters of activities 4.2 kBq, 9.9 kBq and 13 kBq accompanied with a reflective reference surface were positioned at 1 m distance from the detector. Scan was conducted with 10 s integration per point and the angular resolution of the measurement points was 1°. [21]

4.2 Intensified Charge Coupled Device Camera

Andor iStar 320T ICCD-camera has been used in combination with an UV-transmissive objective (UV1228CM, Kogaku) to evaluate the usability of ICCD camera technology in radioluminescence imaging. The photocathode material used in the image intensifier of the camera (WE-AGT. 18-E3) determines the average quantum efficiency of the camera to be 20 % for the radioluminescence signal of nitrogen. [20] The objective has an F/number of 2.8 and a focal length of 12 mm, resulting in an effective aperture of 4.3 mm. It is 80 % transmissive for the UV-wavelengths according to the manufacturer specifications.

In the quantitative experiment, five planchettes with thin layers of Pu-239 evaporated on them were used as emitters. Activities of the planchettes were 106 kBq, 280 kBq, 515 kBq, 2.79 MBq and 5.15 MBq. They were placed in a standard glovebox made of plexiglass, which would attenuate the UV-signal by 80 %. To allow for better transmittance, one of the gloves was removed and the hole was covered with a quartz window. Transmittance of the window was at least 90 % for the radioluminescence signal. The glovebox was covered with two layers of of black rubberized fabric to reduce background illumination. [20] The source-to-detector distance is not specified in the article, but the distance is estimated to have been 80 cm ± 10 cm.

5. COMPARING THE METHODS FOR SENSING THE AIR RADIOLUMINESCENCE

In this section, performance characteristics and general features effecting the usability of the ICCD camera and PMT Scanner are discussed. Background illumination is an important factor when detecting optical signals, and the effect of visible light on the two technologies is analyzed. Factors affecting the time required for executing a measurement are also studied. Lastly, literature results of studies demonstrating the use of the technologies are cited.

5.1 Environmental factors

Background illumination has drastically different effect on the two technologies. As noted in Section 4.1, PMT Scanner is designed to be used with interference filters to greatly attenuate the effects of background illumination of the visible part of spectrum. As a result, the system can be used in illuminated environments mitigating the demand for light shielding of the measurement site. However, any radiation in the operational wavelengths from 330 nm to 350 nm will rapidly deteriorate the sensitivity of the scanner.

Using filters in combination with an ICCD camera to attenuate background illumination has not been demonstrated, although measurements with a filtered EMCCD camera have been conducted [20]. The filtering resulted in losses in the radioluminescence signal, but ghost image of the imaging scene caused by residual background illumination was also suppressed. Signal-to-noise ratio (SNR) of the filtered image was decreased by half compared to the image taken without optical filtering. If optimal sensitivity is required for distinguishing weak sources, care should be taken in shielding the measurement site from any background illumination. Depending on the circumstances, actions required to achieve a good shielding might be time consuming, and in some situations, sufficient shielding might be unattainable.

5.2 Time requirement

Time requirement of a PMT-scanner measurement for different scanning resolutions was studied by taking measurements of 39° by 30° imaging area, similar in size to images produced by 12 mm 2/3" format c-mount lens which is used with the ICCD camera. Scans were carried out with resolutions ranging from 1° to 6° with 1° increments, while integration time was 10 s for each measurement point. Measurement times were calculated for different integration times based on the scans, and the results are presented in Figure 5.1a. From the figure it can be seen that measurement time follows $1/\mathrm{R}^2$ relation, suggesting that considerable time savings are achieved with lower resolutions. Targeting time follows $\sqrt{R}$ relation with resolution, as shown in Figure 5.1b, with goodness of fit of better than 0.99, although wider measurement range would be needed to confirm the relation. Changes of targeting time with resolution are, however, mitigated by the much larger impact of measurement point quantity, which also depends on the resolution.

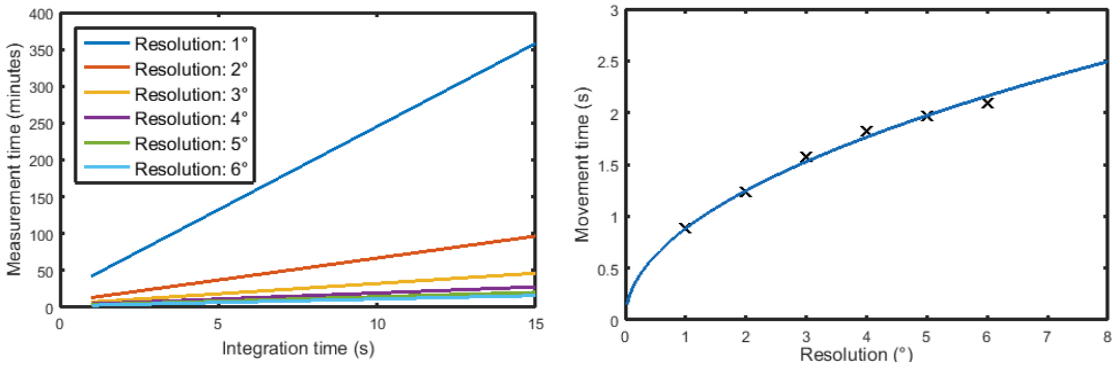

(a) (b)

Figure 5.1 *(a) Relation of total measurement time and integration time per measurement point for different measurement resolutions. When deciding on resolution and measurement time, FOW of the optics should be also taken into consideration for not leaving blind spots on measurement area. (b) Movement time as a function of measurement resolution. Movement time appears to follow $\sqrt{R}$ relation, although wider range of measurements would be needed to confirm the relation with resolution.*

Time required for data acquisition using the PMT Scanner can be calculated by

$$t_{tot} = \frac{\theta\varphi}{R^2}(t_m + t_i) \tag{5.1}$$

where t_{tot} is the total time required, θ and φ are angular width and height of the scan area, respectively, and R is angular resolution of the data points. t_m and t_i are the time required to move the telescope from one acquisition point to the next

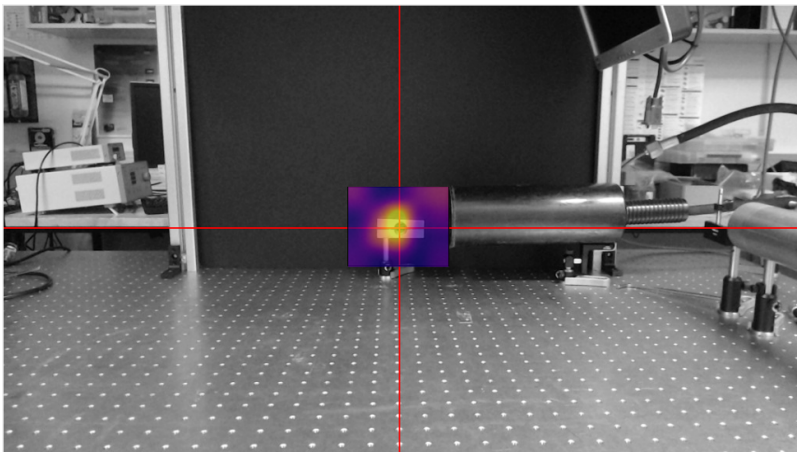

Figure 5.2 *Alpha radiation heat map acquired with PMT Scanner superimposed on a black and white image.*

and the integration time for each measurement point, respectively. Integration time depends on the desired sensitivity of the measurement. Time required to shield the measurement area from UVA-light is another factor that should be considered when planning a measurement.

Time required to acquire a radioluminescence image with an ICCD camera depends on the combination of desired sensitivity and the time needed to ensure adequate conditions for the measurement. As noted in Section 5.1, ICCD camera is considerably more sensitive to background illumination than the PMT Scanner. Therefore, more time and effort may be needed to fulfill the illumination constraints of the ICCD camera than when using the PMT Scanner.

5.3 Minimum Detectable Activity

Minimum detectable activity (MDA) for the PMT Scanner can be estimated using a definition derived by L. A. Currie [5]. When probability for false positive and false negative (α and β) are 5 %, the MDA can be presented as

$$MDA_{PMT} = \frac{L_D}{N_s t_i} = \frac{2.71 + 4.65\sqrt{N_B t_i}}{N_s t_i}, \tag{5.2}$$

where L_D is the net signal level, N_s is the signal count rate and N_B is the background count rate, signal count rate being expressed in counts per time unit per alpha activity. For the detection limit to apply, the observations must be paired, meaning signal and background rates must be measured using the same acquisition time.

With the ICCD camera, MDA can defined to be achieved when a certain SNR requirement is reached. SNR for an ICCD camera can be estimated as

$$SNR = \frac{S}{N} = \frac{P\eta_{pc}t}{\sqrt{F_m^2 t(P\eta_{pc} + N_{EBI})}}, \tag{5.3}$$

where P is the incident photon flux as photons per pixel per second, η_{pc} is the photocathode quantum efficiency, t is the exposure time, F_m is the MCP noise factor and N_{EBI} is the equivalent background illumination for the dark current of the CCD sensor [26]. When photon flux is high enough, effect of equivalent background illumination can be neglected. Now the SNR of an ICCD camera can be expressed as

$$SNR = \sqrt{\frac{P\eta_{pc}t}{F_m^2}}. \tag{5.4}$$

Photon flux P depends on the geometrical efficiency of the measurement setup. Geometrical efficiency is given by the ratio of detector area and the area signal spreads to before a section of it reaches the detector. In the ICCD setup, radioluminescence signal is collected to the image intensifier with a lens, so the detector area equals the effective aperture of the lens. In normal circumstances light spreads spherically to every direction. Geometrical efficiency is therefore given by

$$\Omega = \frac{A_{detector}}{A_{signal}} = \frac{\pi\left(\frac{A_{eff}}{2}\right)^2}{4\pi SDD^2} = \frac{1}{8}\left(\frac{A_{eff}}{SDD}\right)^2, \tag{5.5}$$

where A_{eff} is diameter of effective aperture of the lens. Photon flux P on the sensor can be expressed as

$$P = A_s\Omega\gamma = A_s\frac{1}{8}\left(\frac{A_{eff}}{SDD}\right)^2\gamma, \tag{5.6}$$

where A_s is activity of the source and γ includes all other variables that may affect the photon flux. By including this into the Equation 5.4 we get

$$SNR = \sqrt{\frac{A_s A_{eff}^2 \gamma\eta_{pc}t}{8F_m^2 SDD^2}}, \tag{5.7}$$

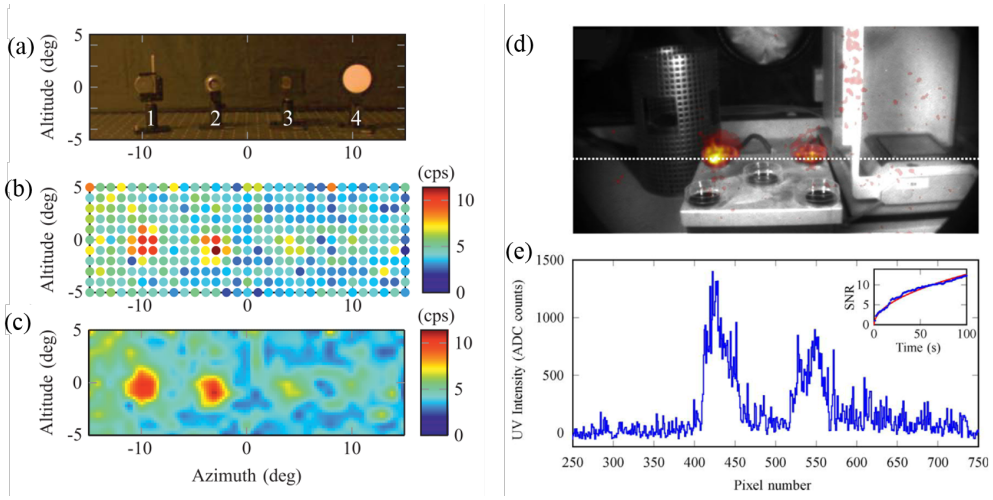

Figure 5.3 *(a) 13 kBq (1), 9.9 kBq (2) and 4.2 kBq (3) alpha sources were scanned while illuminated with yellow fluorescent light. Diffusely reflective surface (4) was used as a reference. (b) Scanned points are shown with the average PMT count rates during the 10 s integration time. (c) Interpolated Radioluminescence heat map reveals the locations of 13 kBq and 9.9 kBq sources. [21] (d) ICCD camera imaging results superimposed on a normal image. (e) Analog to digital converter counts plotted along the dashed line in figure (d). [20]*

from which the source activity A_s, analogous to the MDA of the ICCD for a specific SNR, can be solved:

$$A_s = \frac{SNR^2 F_m^2}{\eta_{pc} t} \frac{8SDD^2}{A_{eff}^2 \gamma} = MDA_{ICCD}. \tag{5.8}$$

In the equation, F_m, η_{pc} and A_{eff} are properties of the camera system, while SDD and exposure time t can be adjusted to best satisfy the imaging circumstances and requirements. Variable γ includes, for example, effects of temperature, pressure and composition of the atmosphere on the photon yield of alpha particles, along with some effects caused by features of the imaging system, like focus plane and transmittance of the lens. Most prominent sources of variance of the MDA_{ICCD} are, however, specified in Equation 5.8.

5.4 Literature results

Quantitative measurements of the PMT Scanner performance have been conducted with experimental arrangement described in Section 4.1. Sand et. al. were able to resolve 9.9 kBq point source with 10 s integration time per measurement point from 1 m distance. 4.2 kBq source was barely detectable. Results of the scan are shown in Figure 5.3a-c, where visualization of measurement data differs from Figure 4.2,

as the former one features newer version of the measurement software. The bialkali PMT of the setup was measured to have a sensitivity of 820 cps/MBq, while the background counts were 4 cps. MDA calculations based on Equation 5.2 and aforementioned sensitivity and background counts suggested the minimum resolvable point source activity to be 4 kBq, corresponding to minimum resolvable surface activity of 0.3 kBq/cm^2. [21]

ICCD camera performance has been demonstrated in an experiment with arrangement similar to description in Section 4.2. The image was acquired by combining one hundred 1 s exposures from a scene with all five emitters. Gain of the ICCD camera was set to 3644. The resulting radioluminescence image superimposed over an image taken under normal lighting is presented in Figure 5.3 (d). Averages of three vertically neighbouring pixels were calculated along the dashed line and are presented in Figure 5.3 (e). The 5.15 MBq and 2.79 MBq sources can be distinguished from the image. Some light leaks can also be seen on bright surfaces on the right side of the image. Cumulative SNR of the 1 s exposures was calculated with a similar method as was used by Lamadie et al. [13]. The results are plotted along with best fit lines indicating the $\sqrt{t}$ dependence of the SNR. The SNR achieved after total exposure of 100 s was 14. [20]

6. PERFORMANCE ANALYSIS

Performance of ICCD camera and PMT Scanner for radioluminescence signal detection are next compared based on the literature results presented in Section 5.4. In the comparison, a reference imaging area of 39° by 30° is used. For the comparison, MDA for the ICCD must first be defined. This can be achieved by first solving the unknown variables F_m, η_{pc} and γ from the Equation 5.4 for the values of SNR, SDD, A_s, A_{eff} and t of the experimental setup of Section 5.4:

$$\mu = \frac{8F_m^2}{\eta_{pc}\gamma} = \Big(\frac{A_{eff}}{SNR \cdot SDD}\Big)^2 A_s t \tag{6.1}$$

The solved unknown variables of the ICCD setup are assumed to stay constant and to be independent from any known variables. Resulting equation for the MDA for a specific SNR is

$$MDA_{ICCD} = \mu\Big(\frac{SNR' \cdot SDD'}{A'_{eff}}\Big)^2 \frac{1}{t'}, \tag{6.2}$$

where SDD', A_{eff}' and t' are free variables dictated by the simulated scenario and SNR' is determined by the reguired confidence level of detection.

MDA for the ICCD camera is calculated for SDD of 1 m, equal to the SDD of PMT Scanner setup. SNR of 3 was used in the MDA calculation, which is analogous with confidence level of 3 σ for detecting a source with activity equal to the MDA. Effect of more efficient lens with an F number of 1.4, compared to the F/2.8 lens of the experiment, and similar focal length of 12 mm is also simulated. C-mount lenses with focal length of 12 mm and F/1.4 are readily available, but most of them are not transmissive to UV-light. Disadvantages of a lens with better light collection efficiency would be a shallower focal plane and slightly more distorted image. These, however would not significantly affect radioluminescence imaging as the the illuminating hemisphere does not have clear boundaries if the imaging is done in exposed space with no obstacles near the alpha source.

Measurement conditions and PMT Scanner performance are assumed to be similar to the ones presented in Section 5.4. MDA and measurement time are calculated for different resolutions and integration times with Equations 5.2 and 5.1. Movement time and number of measurement points were estimated for a resolution of 1.7°, which is the minimum resolution still capable to cover whole measurement area without blind spots for the FOW of 2.5° of the Scanner optics.

PMT Scanner performance was also simulated for a measurement sequence utilizing continuous horizontal movement. In this method, PMT counts are continuously recorded while the FOW of the system moves horizontally at constant speed from one side of the measurement area to the other. For most scenarios, multiple passes must be recorded with different tilt angles to fully cover the vertical span of the measurement area. Integration time of this method is a function of the slew speed, the smallest horizontal length of the FOW and the number of passes. For a circular FOW, the horizontal length becomes shorter near the edges, requiring slower slew speed for a certain integration time to be achieved. The horizontal passes can, however, be overlapped, allowing for faster slew speed. This way, the horizontal spans of the FOW for the overlapping passes are effectively summed on the overlapping area. Simulation was done with the number of horizontal passes ranging from 12 to 20, the smallest number being the minimum for fully covering the vertical span of the measurement area. The difference in the number of passes results in different amounts of overlap and different slew speeds, ultimately affecting the total measurement time. The number of lines resulting in shortest measurement time was found to be 16, leading to 0.7° of overlap and 67 min measurement time for 10 s integration time over the whole measurement area.

All the results are presented in Figure 6.1. It can be seen that the continuous horizontal movement of the PMT Scanner with 0.7° vertical overlap performs better than the movement used in experimental setup with 1.7° resolution. The 2° resolution is quicker than the continuous horizontal movement for integration times of 11 s and longer. The disadvantage of the 2° resolution measurement is that, when used with optics with 2.5° FOW, it leaves some areas between the measurement points unmeasured, providing that the FOW is assumed to be circular in shape. This is illustrated in Figure 6.2. The ICCD setup with F/2.8 lens seems to be slower than the PMT Scanner, except when the PMT Scanner is operated with 1° resolution. However, the benefits of oversampling with the PMT Scanner have not been studied. The simulation of ICCD camera with F/1.4 lens suggests better performance for the PMT Scanner when detecting sources with activities higher than 11 kBq. The ICCD surpasses the performance of the PMT Scanner between 5 kBq and 11 kBq, considering the possible error in the ICCD results caused by the uncertainty in the

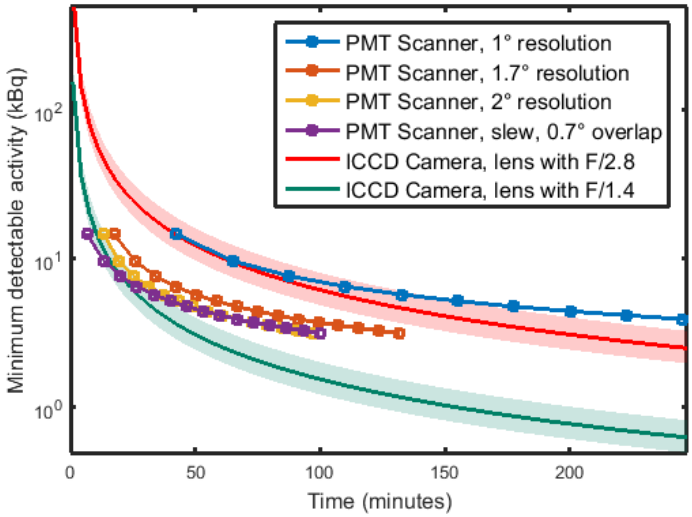

Figure 6.1 *MDA values plotted as a function of the total measurement time for PMT Scanner with three different resolutions and for simulated ICCD setup with SDD of 1 m. Data points of PMT Scanner curves begin from 1 s integration and continue with 1 s increments. Shaded areas above and below the ICCD camera curves correspond the error caused by the uncertainty in the SDD of the original measurement.*

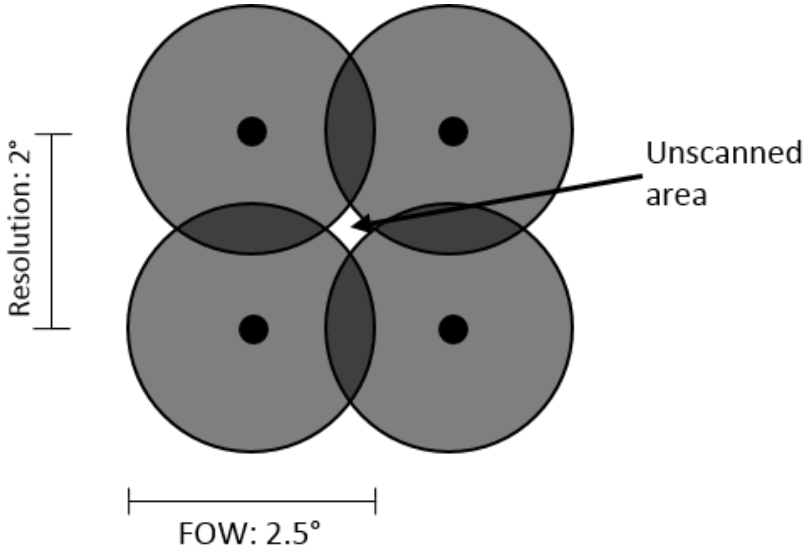

Figure 6.2 *With 2.5° FOW and 2° resolution, some areas may be left unscanned.*

SDD in the original measurement. For lower MDAs than 5 kBq, ICCD camera appears to perform better than the PMT Scanner. Detecting such activities require measurement times longer than 38 minutes.

Based on the simulation results, guidelines can be established to determine the best measurement technology for different measurement scenarios. These guidelines are presented in Table 6.1. The simulation also emphasizes the significance of lens performance for the ICCD camera measurement, pointing out the components with

	MDA $\leq$ 5 kBq	MDA $>$ 11 kBq
No background illumination	ICCD camera	PMT Scanner
UV-free background illumination	PMT Scanner	PMT Scanner

Table 6.1 *Recommended detector technology for different measurement conditions.*

biggest potential for improvements in the future. However, measurements with the two technologies need to be conducted in comparable measurement conditions to evaluate the validity of the simulations. Most notably, the assumption that MCP noise factor F_m, photocathode quantum efficiency η_{pc} and unknown variables included in γ in Equation 6.2 stay constant over wide range of integration times and source activities, may cause considerable inaccuracies in the results.

7. CONCLUSIONS

Aim of the thesis was to compare the performance of PMT Scanner and ICCD camera for radioluminescence signal detection. Results of previously conducted measurements were used as basis for the simulation of the systems. The relation of minimum detectable activity and measurement time was the main focus in the simulation. Results show that, if the ICCD camera is combined with a 12 mm F/2.8 lens, the PMT Scanner is able to detect sources with smaller activities than the ICCD camera for the studied range of measurement times between 0 and 150 minutes. ICCD camera was also simulated with a 12 mm F/1.4 lens. With the more efficient lens, ICCD cameras detection performance surpasses the performance of the PMT Scanner for longer than 20 minute measurement times. In good measurement conditions, both systems are capable of detecting 8 kBq sources in the 20 minute measurement time.

Efficiency of the optics was found to be an important factor for the ICCD camera performance. According to the simulation, new UV transmissive optics with larger effective aperture would significantly improve the detection limits of the ICCD camera. Lenses with F/1.4 and good image quality, although not transmissive to UV wavelengths, are readily available. For radioluminescence imaging applications, image quality and minimum distortion are of less importance compared to most other applications, which would probably allow for even larger effective aperture to be achievable.

For the PMT Scanner a continuous scan method was found to be significantly faster than the currently used movement system. Another approach for achieving shorter measurement times could be optimizing the field of view of the optics. For close range measurements, similar spatial resolution would be achieved with a wider field of view than for long range measurements with a narrower field of view. This would result in fewer measurement points and overall shorter measurement time.

Simulation results still need to be confirmed by actual measurements due to the assumptions made in the simulation. The error margins of the ICCD results, caused by the uncertainty of the imaging distance in the measurement the simulation is based on, impair the usability of the results when trying to determine the better

detector technology. However, for glovebox imaging, the ICCD camera emerges as the preferable technology in most circumstances, providing that proper light shielding is easily achievable. In practice, proper and effortless shielding would require substantial modifications to be made to the glove boxes. When total darkness cannot be ensured, but absence of UV light can be guaranteed, the PMT Scanner is the only usable option among the two technologies. That's because a filter stack with adequate attenuation would decrease the signal to an insufficient level for the ICCD camera.

BIBLIOGRAPHY

[1] Andor Corporation, "Intensified ccd cameras," https://andor.oxinst.com/learning/view/article/intensified-ccd-cameras, accessed: 09.11.2018.

[2] P. P. Bachelor, D. V. Jordan, W. W. Harper, B. D. Cannon, and E. C. Finn, "Self-absorption effects on alpha-induced atmospheric nitrogen fluorescence yield," *Journal of Radioanalytical and Nuclear Chemistry*, vol. 282, no. 3, pp. 873–876, 2009.

[3] S. M. Baschenko, "Remote optical detection of alpha particle sources," *Journal of Radiological Protection*, vol. 24, no. 1, pp. 75–82, 2004.

[4] I. P. Csorba, *Image Tubes*. Indianapolis, Indiana: Howard W. Sams & Co., 1.3.1985.

[5] L. A. Currie, "Limits for qualitative detection and quantitative determination. application to radiochemistry," *Analytical chemistry*, vol. 40, no. 3, pp. 586–593, 1968.

[6] T. Gys, "Micro-channel plates and vacuum detectors," *Nuclear Instruments and Methods in Physics Research, Section A: Accelerators, Spectrometers, Detectors and Associated Equipment*, vol. 787, pp. 254–260, 2015. [Online]. Available: http://dx.doi.org/10.1016/j.nima.2014.12.044

[7] Hamamatsu Photonics, "Photomultiplier Tubes," 2007, accessed: 2.12.2018. [Online]. Available: https://www.hamamatsu.com/resources/pdf/etd/PMT_handbook_v3aE.pdf

[8] W. Huggins and L. Huggins, "Further Observations on the Spectrum of the Spontaneous Luminous Radiation of Radium at Ordinary Temperatures," *Proceedings of the Royal Society of London (1854-1905)*, vol. 72, pp. 409–413, 1903. [Online]. Available: http://dx.doi.org/10.1098/rspl.1903.0070

[9] IAEA, "Status of the Decommissioning of Nuclear Facilities Around the World," p. 135, 2004, accessed: 16.12.2018. [Online]. Available: https://www-pub.iaea.org/MTCD/Publications/PDF/Pub1201_web.pdf

[10] S. Ihantola, J. Sand, K. Peräjärvi, J. Toivonen, and H. Toivonen, "Fluorescence-assisted gamma spectrometry for surface contamination analysis," *IEEE Transactions on Nuclear Science*, vol. 60, no. 1, Feb. 2013.

[11] E. Inrig, V. Koslowsky, B. Andrews, M. Dick, P. Forget, H. Ing, R. Hugron, and L. Wong, "Development and testing of an air fluorescence imaging system for the detection of radiological contamination," in *AIP Conference Proceedings*, vol. 1412, no. 1. American Institute of Physics, dec 2011, pp. 393–400. [Online]. Available: http://aip.scitation.org/doi/abs/10.1063/1.3665340

[12] T. Kerst and J. Toivonen, "Intense radioluminescence of no/n2-mixture in solar blind spectral region," *Opt. Express*, vol. 26, no. 26, pp. 33 764–33 771, Dec 2018. [Online]. Available: http://www.opticsexpress.org/abstract.cfm?URI=oe-26-26-33764

[13] F. Lamadie, F. Delmas, C. Mahe, P. Girones, C. Le Goaller, and J. Costes, "Remote alpha imaging in nuclear installations: New results and prospects," *IEEE transactions on nuclear science*, vol. 52, no. 6, pp. 3035–3039, 2005.

[14] N. Matuschek, F. X. Kartner, and U. Keller, "Theory of double-chirped mirrors," *IEEE Journal of Selected Topics in Quantum Electronics*, vol. 4, no. 2, pp. 197–208, March 1998.

[15] R. Paschotta, "Dielectric mirrors," Oct 2017. [Online]. Available: https://www.rp-photonics.com/dielectric_mirrors.html

[16] S. V. Polyakov, *Photomultiplier Tubes*. Elsevier Inc., 2013, vol. 45. [Online]. Available: http://dx.doi.org/10.1016/B978-0-12-387695-9.00003-2

[17] J. Sand, S. Ihantola, K. Peräjärvi, H. Toivonen, and J. Toivonen, "Radioluminescence yield of alpha particles in air," *New Journal of Physics*, vol. 16, 2014.

[18] J. Sand, *Alpha Radiation Detection via Radioluminescence of Air*, ser. Tampere University of Technology. Publication. Tampere University of Technology, 12 2016.

[19] J. Sand, V. Hannuksela, S. Ihantola, K. Peräjärvi, H. Toivonen, and J. Toivonen, "Remote optical detection of alpha radiation," in *Optics Days 2011, May 12-13, Oulu*, ser. Optics Days. Finnish Optical Society FOS, 2011.

[20] J. Sand, S. Ihantola, K. Peräjärvi, A. Nicholl, E. Hrnecek, H. Toivonen, and J. Toivonen, "Imaging of alpha emitters in a field environment," *Nuclear Instruments and Methods in Physics Research, Section A: Accelerators, Spectrometers, Detectors and Associated Equipment*, vol. 782, pp. 13–19, 2015.

[21] J. Sand, A. Nicholl, E. Hrnecek, H. Toivonen, J. Toivonen, and K. Peräjrvi, "Stand-Off Radioluminescence Mapping of Alpha Emitters under Bright Lighting," *IEEE Transactions on Nuclear Science*, vol. 63, no. 3, pp. 1777–1783, 2016.

[22] Stanford Computer Optics Inc, "The image intensifier," accessed: 09.11.2018. [Online]. Available: https://stanfordcomputeroptics.com/technology/image-intensifier.html

[23] C. I. Thompson, E. E. Barritt, and C. Shenton-Taylor, "Predicting the air fluorescence yield of radioactive sources," *Radiation Measurements*, vol. 88, pp. 48–54, 2016.

[24] P. A. Tipler and R. A. Llewellyn, *Modern physics, More Chapter 11, Energetics of Alpha Decay.* W.H. Freeman and Co., 2012.

[25] T. Waldenmaier, J. BlÃmer, and H. Klages, "Spectral resolved measurement of the nitrogen fluorescence emissions in air induced by electrons," *Astroparticle Physics*, vol. 29, no. 3, pp. 205 – 222, 2008. [Online]. Available: http://www.sciencedirect.com/science/article/pii/S0927650508000145

[26] W. Zhang and Q. Chen, "Signal-to-noise ratio performance comparison of electron multiplying ccd and intensified ccd detectors," in *2009 International Conference on Image Analysis and Signal Processing*, April 2009, pp. 337–341.